# Enabling Magnesium Anodes by Tuning the Electrode/Electrolyte Interfacial Structure

*Xiaoyu Wen,[1] Zhou Yu,[2,3] Yifan Zhao,[4] Jian Zhang,[4] Rui Qiao,[5] Lei Cheng,[2,3]* Chunmei Ban,[6]* Juchen Guo,[1,4]**

[1]Department of Chemical and Environmental Engineering and [4]Materials Science and Engineering Program, University of California, Riverside, CA 92521, United States

[2]Joint Center for Energy Storage Research and [3]Materials Science Division, Argonne National Laboratory, Lemont, IL 60439, United States

[5]Department of Mechanical Engineering, Virginia Tech, Blacksburg, VA 24061, United States

[6] Paul M. Rady Department of Mechanical Engineering, University of Colorado Boulder, Boulder, CO 80309, United States

**KEYWORDS:** interface, magnesium anode, magnesium ion batteries, $Mg(TFSI)_2$ , NaTFSI

**ABSTRACT:** A new deposition mechanism is presented here to ensure highly reversible stripping and plating of magnesium (Mg) anode for Mg-ion batteries. It is known that the reduction of electrolyte anions such as bis(trifluoromethanesulfonyl)imide (TFSI) ions causes the surface passivation at the Mg surface, resulting in poor electrochemical performance for Mg-metal batteries. We reveal that the addition of sodium cation ($Na^+$) in Mg-ion electrolytes, can

fundamentally alter the interfacial chemistry and structure at the Mg anode surface. The molecular dynamics simulation suggests that $Na^+$ cations contribute to a significant population in the interfacial double layer so that $TFSI^-$ anions are excluded from the immediate interface adjacent to the Mg anode. As a result, the $TFSI^-$ decomposition is largely suppressed so does the formation of passivation layer at the Mg surface. Furthermore, such interfacial chemistry change results to a new Mg deposition mechanism, in which Na is first deposited as a transit species enabled by the existing overpotential, followed by Mg deposition from displacement reaction (i.e. chemical reduction by Na). This mechanism is supported by our electrochemical, microscopic, and spectroscopic analyses. The resultant Mg deposition demonstrates smooth surface morphology and lowered overpotential comparing to the pure $Mg(TFSI)_2$ electrolyte.

## TOC Graphic

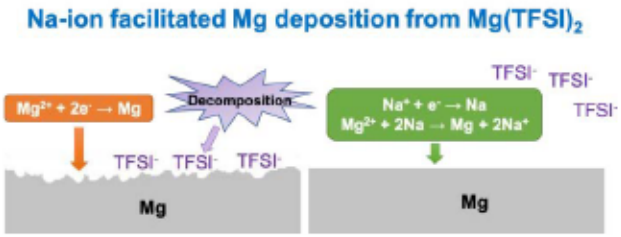


## INTRODUCTION

Rechargeable magnesium (Mg) batteries have been investigated as one of the alternatives to lithium-ion batteries to meet the soaring demand for energy storage technologies. Despite numerous research efforts, the lack of benchmark Mg electrolytes is still a main obstacle for the development of practical rechargeable Mg batteries.[1,2] In addition to the conventional Mg-Cl complex electrolytes, Mg-ion electrolytes based on weakly coordinating anions received increasing attention in recent years due to their non-corrosive nature and higher anodic stability.

To date, the selection of anions is very limited: Perchloride ($ClO_4^-$) is not compatible with Mg anode due to its proneness to reductive decomposition;[3] Hexafluorophosphate ($PF_6^-$) has low solubility in ethereal solvents and can also passivate the Mg anode.[4] On the other hand, Mg-ion electrolytes based on non-conventional weakly coordinating anions, represented by 10- or 12-vertex carborane[5-8] and tetrakis(hexafluoroisopropylozy)borate,[9] has been proven to be compatible with Mg anode and exhibit remarkable anodic stability.[10] Unfortunately, the complicated preparation and low repeatability hinder the wide deployment of these electrolytes. Among all Mg-ion electrolytes with weakly coordinating anion, the ones using bis(trifluoromethanesulfonyl)imide ($TFSI^-$) anion probably received most of the studies to date. The advantage of $Mg(TFSI)_2$ is being readily available and highly soluble in a large variety of solvents. However, its disadvantage is detrimental: the $TFSI^-$ anion is prone to cathodic decomposition to form passivation layers composed of extremely insulating fluoride, sulfide, and oxide species, which leads to large overpotential for Mg deposition-stripping and inferior structure of the Mg deposit.[11] The performance of Mg anode in $Mg(TFSI)_2$ electrolyte can be improved by adding magnesium chloride ($MgCl_2$). However, the resultant electrolyte is no longer the "simple salt" type since the cations become monovalent Mg-Cl complexes.[12] Also, introducing corrosive chloride in the electrolyte decreases the anodic stability and compatibility with high voltage metal oxide materials.[13] Therefore, the current $Mg(TFSI)_2$ electrolytes are not feasible for practical Mg-ion batteries.

Passerini and co-workers[14, 15] studied the effects of cation (including monovalent ions $Li^+$, $Na^+$ as well as bivalent ions $Mg^{2+}$, $Zn^{2+}$) coordination on the reductive stability of the $TFSI^-$ anion. Their Raman spectroscopic characterization and molecular dynamics (MD) simulations showed that the coordination number of $TFSI^-$ anion with divalent $Mg^{2+}$ and $Zn^{2+}$ is higher than that with

monovalent $Li^+$, $Na^+$. The cation-anion residence times for $Mg^{2+}$ and $Zn^{2+}$ are also longer than those with $Li^+$ and $Na^+$. These results indicate significantly faster dissociation kinetics of the TFSI salts with monovalent cations in solution due to their lower cation-anion binding energy.

Based on these findings, we hypothesize that adding a small number of monovalent cations such as $Na^+$ can change the structure of the Mg/electrolyte interface, thus altering the mechanism of Mg deposition: Under reductive environment, the monovalent cations can migrate to the Mg anode surface and contribute to the double layer due to their higher transference number comparing to $Mg^{2+}$.[16] As a result, fewer $TFSI^-$ anions should exist at the interface due to the fast dissociation with the monovalent cations. In addition to the exclusion of $TFSI^-$ anions from the interface, $Na^+$ cation as the additive (instead of $Li^+$) may offer another benefit. The reduction potential of $Na^+$/Na (standard potential at -2.71 V vs. SHE) is only slightly lower than that of $Mg^{2+}$/Mg (standard potential at -2.38 V vs. SHE).[17] Therefore, we hypothesize that the overpotential during Mg deposition can enable transit Na deposition, which in turn can deposit Mg via chemical reduction of $Mg^{2+}$ cation. This hypothesized process is expected to alleviate the electrochemical decomposition of $TFSI^-$ anion as well reduce the effective overpotential, thus leading to the improved performance of Mg anode.

## EXPERIMENTAL SECTION

**Electrolyte Preparation:** Due to the sensitivity to air and moisture, all manipulations were undertaken in an argon-filled glovebox (<0.1 ppm $H_2O$ and $O_2$). Magnesium bis(trifluoromethane-sulfonyl)imide ($Mg(TFSI)_2$, 99.5%) and sodium bis(trifluoromethane-sulfonyl)imide (NaTFSI, 99.5%) were purchased from Solvionic (France) and dried under vacuum for 24h at 100 °C prior to use. Anhydrous 1,2-Dimethoxyethane (DME, 99.5%, inhibitor-free) was purchased from

Sigma-Aldrich, and further dried with 3Å molecular sieves. The water content of electrolytes was monitored by Karl Fischer and kept no higher than 15 ppm.

**Electrochemical Analyses:** All electrochemical experiments were performed in the argon-filled glovebox using a Gamry potentiostat/galvanostat/ZRA (Reference 3000) at room temperature. Cyclic voltammetry (CV) was carried out in a Gamry three-electrode cell with a platinum (Pt) working electrode (3mm disc, Gamry) and two Mg plates (0.25 mm, 99.9%, Alfa Aesar) as reference electrode and counter electrode, respectively. The Pt working electrode was polished with alumina particles (0.05 μm) water dispersion on polishing pad and sonicated in ethanol, and then dried under vacuum before each experiment. The Mg reference and counter electrodes were scratched with stainless steel blaze to remove surface passivation layer in glovebox prior to every experiment. Working electrode with detachable Pt disk was used in the chronopotentiometry Mg deposition experiments. The Pt electrode was detached after the deposition for scanning electron microscopic analysis. The pretreatment of electrodes was as same as that in the CV experiments. The Electrochemical Quartz Crystal Microbalance (EQCM) measurements were carried out in a PTFE Gamry QCM cell using the potentiostat combined with a Gamry eQCM 10M™ Quartz Crystal Microbalance. 10 MHz Pt-coated Crystal was used as working electrode (with an electrode area of 0.205 $cm^2$) to measure the mass change. Two Mg plates were used as the reference and counter electrodes, respectively. The mass change of the electrode can be calculated by using the Sauerbrey equation:

$$\Delta m = -\frac{\Delta f}{C_f}$$

where $\Delta f$ is the measured resonant frequency (Hz), $C_f$ is the mass sensitivity factor which is equal to 226 Hz $cm^2$ $ug^{-1}$ for 10 MHz Crystal, obtained from standard copper deposition experiment.

**Surface Characterizations:** The sample was first rinsed with anhydrous DME three times to remove the residue of the reactants, followed by evaporating the solvent on a hotplate at 80 °C for 10 mins inside the argon-filled glovebox. X-ray photoelectron spectroscopy (XPS) was conducted with a high sensitivity Kratos AXIS Supra with monochromatic Al(Kα) radiation (1486.7 eV). The emission current for excitation was 15 mA. The etching of the sample for depth profiling measurements was performed with 5 keV $Ar^+$ sputtering. All XPS spectra were analyzed by the CasaXPS software using the carbon 1s peak at 284.8 eV (adventitious carbon) as the reference. The XPS samples were transferred and loaded under continuous argon protection without exposure to ambient environment. The surface morphology and elemental composition of samples were characterized with scanning electron microscopy (SEM, Nova Nano S450) and energy dispersive X-ray (EDX) spectroscopy.

**Molecular Dynamics Simulations** were performed using GROMACS package.[18] Pre-test simulations have been performed on two bulk electrolytes composed of salt and solvent molecules as shown in Table 1 to determine the bulk density under the NPT ensemble. The pressure was maintained at 1 atm using the Parrinello-Rahman barostat for the NPT ensemble.[19, 20] Then, the simulations composed of electrodes and electrolytes have been conducted in the NVT ensemble. The OPLS-aa force fields were used for liquid electrolytes.[21, 22] The electrode atoms were modeled as $sp^2$ carbon with the same Lennard-Jones parameters in the Amber force fields.[23] These generic force fields have been recently utilized to investigate the electrical double layer in liquid electrolytes.[24] Considering the EDL structure may be sensitive to the force field, we performed another set of simulations with the recently developed Lennard-Jones parameters for the $Na^+$ and $Mg^{2+}$ ion.[25] The simulation timestep is 2 fs and the temperature is 353 K, which is lower than the boiling point of DME. This elevated temperature can facilitate effective sampling. The system

temperature was maintained using the velocity rescaling thermostat.[26] The cutoff length for the non-electrostatic interactions is 1.2 nm. The electrostatic interactions were computed using the particle mesh Ewald (PME) method with slab correction in the *z*-direction.[27] The real space cutoff and fast Fourier transform spacing were set to 1.2 and 0.12 nm, respectively. Pre-test simulations were run for 30 ns and the last 10 ns stable trajectories were used to calculate the bulk density of the electrolytes. For the formal simulations, 20 ns equilibration was followed by a 100 ns production run.

**DFT Calculations:** The molecular structures of Na-TFSI and Mg-2TFSI were optimized at the DFT level with the B3LYP/6-31G(d,p) method at gas phase and CPCM continuum model[28] using the Gaussian program.[29] Given that dichloroethane and DME have a similar shape and dielectric constant, dichloroethane was used as the solvent in the implicit continuum calculation instead of DME, which is not a standard solvent in the Gaussian program.[29, 30] The $Na^+$ and $Mg^{2+}$ ion was placed on different position of the $TFSI^-$ ion to explore the most stable adsorption structure. The binding energy (BE) between cation and anion was defined as $BE_{Cation/Anion} = E_{Cation+Anion} - E_{Cation} - E_{Anion}$, where $E_{Cation}$, $E_{Anion}$, and $E_{Cation+Anion}$ is the energy of cation, anion, and the total system, respectively.

## RESULTS AND DISCCUSION

To illustrate the effect of $Na^+$ cation in the $Mg(TFSI)_2$ electrolyte, the electrochemical properties of a conventional electrolyte composed of 0.5 M $Mg(TFSI)_2$ in 1,2-dimethoxyethane (DME) (referred as the Mg electrolyte) is compared to an electrolyte composed of 0.5 M $Mg(TFSI)_2$ and 0.1 M NaTFSI in DME (referred as the Mg/Na electrolyte). **Figure 1a** shows the cyclic voltammetry (CV) curves obtained from these two electrolytes from -1.5 V to 3.0 V versus Mg at

25 mV $s^{-1}$. The onset potential of Mg deposition in the pure Mg electrolyte is -1.0 V; on the other hand, the onset potential of reductive current in the Mg/Na electrolyte is approximately -1.3 V (both versus Mg). More interestingly, at the beginning stage of the anodic scan, the Mg/Na electrolyte clearly shows a reductive current starting at -1.4 V and peaked at -1.3 V versus Mg. This reductive current peak in the anodic scan is strong evidence for a spontaneous chemical reduction reaction occurred on the working electrode. This observation is consistent with our hypothesis that Na is first deposited and consequentially reduces $Mg^{2+}$ to Mg metal. The chronopotentiometry curves in **Figure 1b** display the different deposition behaviors in these two electrolytes under a realistic areal current at 0.5 mA $cm^{-2}$ (deposition curve at 1.0 mA $cm^{-2}$ is in **Figure S1** in the Supporting Information). The pure Mg electrolyte demonstrates a stable Mg deposition at -0.75 V versus Mg, which is in agreement with the previous report.[8] The Mg/Na electrolyte displays a distinctly different behavior with a unique jagged deposition curve throughout the entire deposition period of 20 hours with an average potential at -0.6 V versus Mg. The fluctuation of the potential curve is composed of cycles of potential increase and decrease, which is consistent with the proposed Na deposition and consequential chemical reduction of $Mg^{2+}$ to form Mg metal.

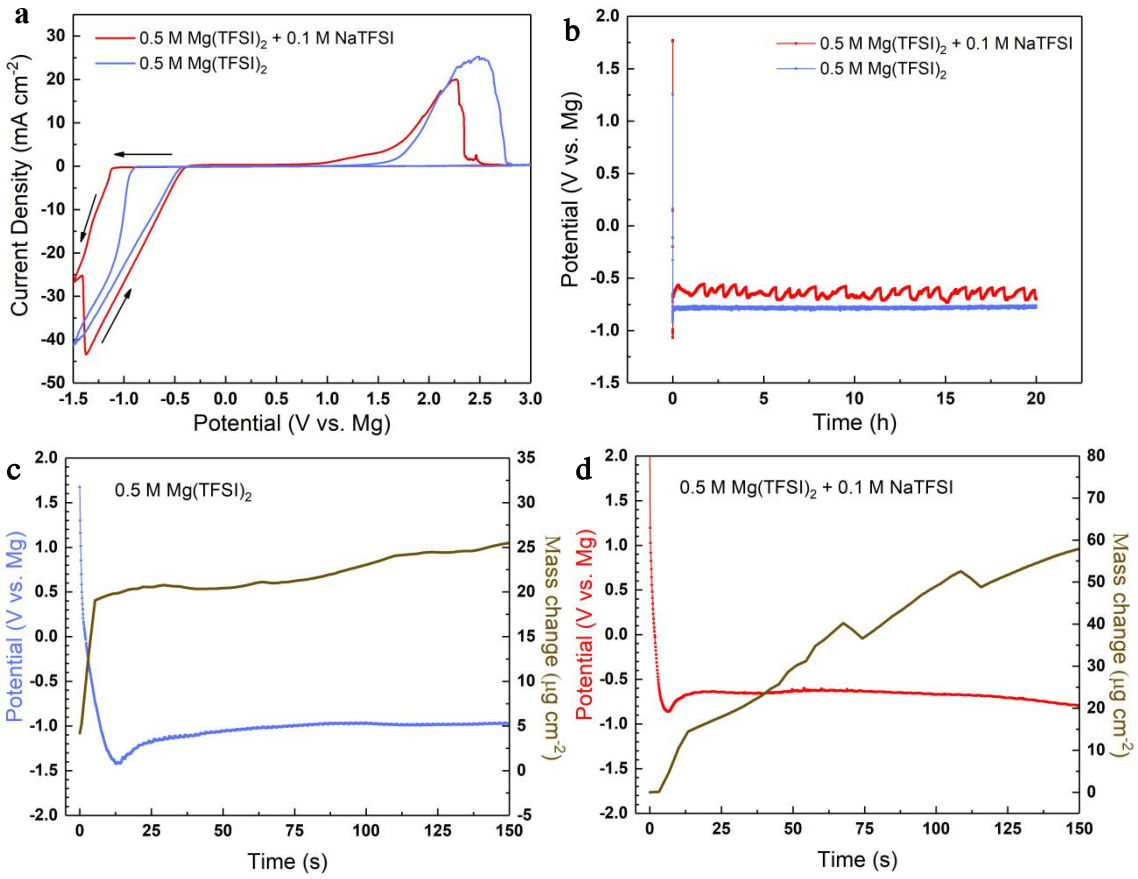


**Figure 1.** (a) CV curves at 25 mV $s^{-1}$ and (b) chronopotentiometry deposition curves at 0.5 mA $cm^{-2}$ in the Mg and Mg/Na electrolytes; EQCM deposition potential and mass change as the function of time at 0.5 mA $cm^{-2}$ in (c) pure Mg electrolyte and (d) Mg/Na electrolyte.

The subtle electrode process is then probed with the electrochemical quartz crystal microbalance (EQCM) experiments using a Pt-coated crystal electrode (cell parameter calibrated with standard copper electrodeposition). EQCM technique is known to be capable of accurately measuring the change of mass on the electrode during an electrochemical process.[31, 32] **Figures 1c** and **1d** show the simultaneous mass change on the electrode during the deposition process with a current of 0.5 mA $cm^{-2}$. The mass change demonstrates drastically different patterns in these two electrolytes. After the initial step-wise mass gain observed in both electrolytes due to the formation of double

layer,[33, 34] the rate of mass gain in the pure Mg electrolyte is much slower than that in the Mg/Na electrolyte. The mass of the deposition (after the adsorption of the interface layer) is approximately 7 μg $cm^{-2}$ in the Mg electrolyte after 150 seconds; meanwhile, the mass of the deposition in the Mg/Na electrolyte is about 45 μg $cm^{-2}$, which evidences more effective deposition.

The surface characterizations provide direct evidence of superior Mg deposition from the Mg/Na electrolyte. **Figure 2a** and **2b** are the scanning electron microscopy (SEM) images of the Mg deposition from the pure Mg electrolyte and Mg/Na electrolyte under 0.5 mA $cm^{-2}$, respectively (The SEM images of Mg deposited under 1 mA $cm^{-2}$ are in **Figure S2** in the Supporting Information). Consistent with the previous report,[8] the Mg deposited from the Mg electrolyte has a porous and uneven surface due to the severe decomposition of $TFSI^-$ anions. In contrast, Mg deposition with a smooth surface was obtained from the Mg/Na electrolyte, indicating significantly alleviated decomposition of $TFSI^-$ anions. The energy dispersive X-ray spectra in the Supporting Information (**Figure S3**) indicate higher Mg content and lower content of fluorine (F) and sulfur (S) in the Mg deposited from the Mg/Na electrolyte.

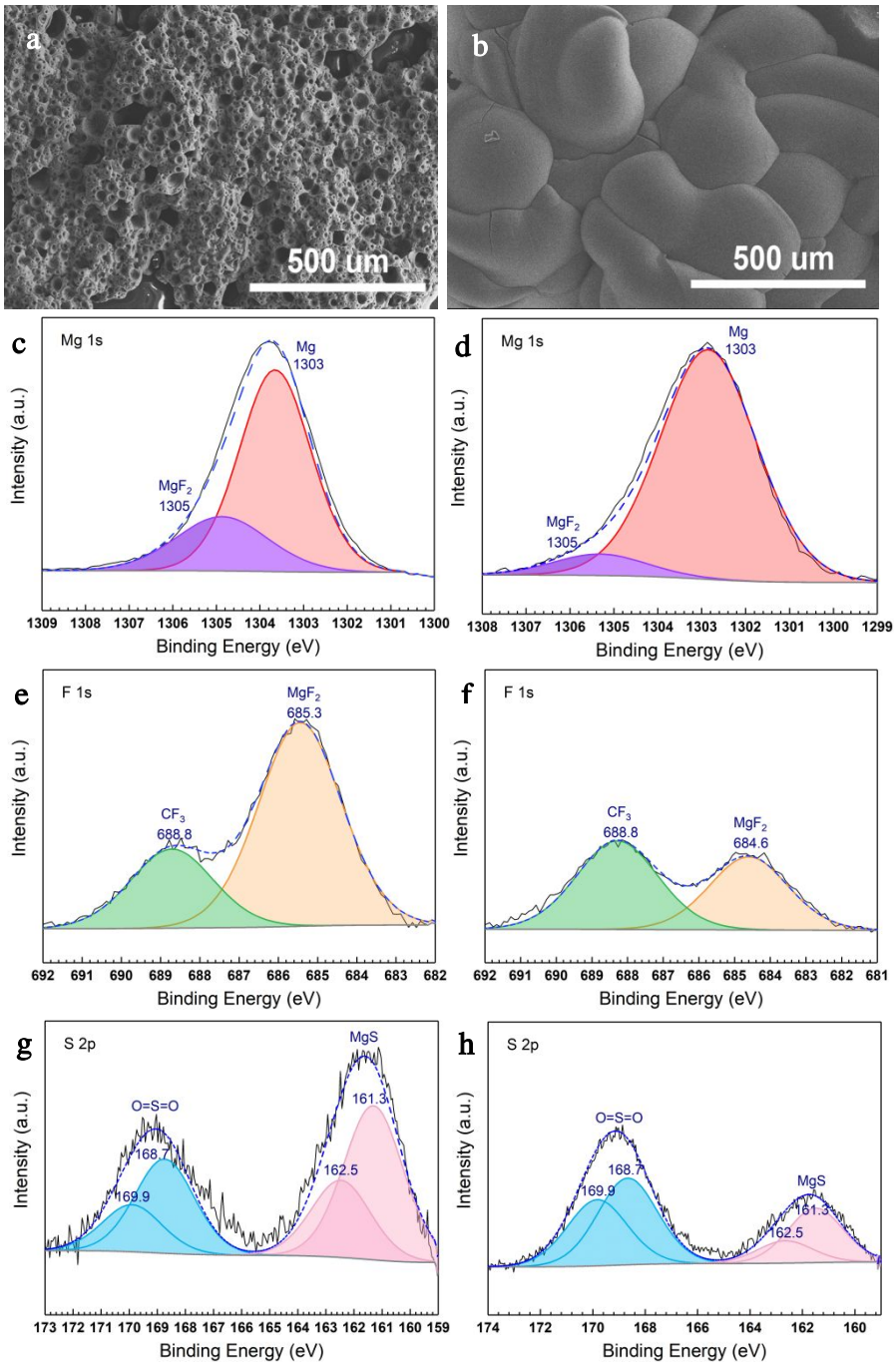


**Figure 2.** SEM images of the Mg deposition on Pt electrode from the (a) pure Mg electrolyte and (b) Mg/Na electrolyte; (c) Mg 1s, (e) F 1s, and (g) S 2p XPS spectra of the Mg deposition surface from the pure Mg electrolyte; (d) Mg 1s, (f) F 1s, and (h) S 2p XPS spectra of the Mg deposition surface from the Mg/Na electrolyte.

The surface composition of the Mg deposition was further analyzed by X-ray photoelectron spectroscopy (XPS). **Figures 2c**, **2e**, and **2g** are the XPS spectra of the Mg surface deposited from the pure Mg electrolyte; and **Figures 2d**, **2f**, and **2h** are the spectra of the Mg surface deposited from the Mg/Na electrolyte. The peak at 1303 eV in the Mg 1s spectra is attributed to the metallic Mg[35] and the peak at 1305 eV is attributed to the oxidized Mg due to the formation of Mg fluoride, Sulfide, and oxide from the decomposition of $TFSI^-$.[36] The XPS peak ratio of $Mg/Mg^{2+}$ in the Mg/Na electrolyte is significantly higher than that in the pure Mg electrolyte, indicating that $TFSI^-$ decomposition is significantly reduced in the former. The 688.8 eV peak in the F 1s spectra (Figure 2e and 2f) is attributed to the $CF_3$ group in the residual $TFSI^-$ anion;[37] and the 684.6 eV F 1s peak represents fluoride due to the formation of $MgF_2$.[38] Using the $CF_3$ peak as the reference, it is clear that the peak intensity of $MgF_2$ in the pure Mg electrolyte is much higher than that in the Mg/Na electrolyte. A similar observation can be made in S 2p spectra in Figures 2g and 2h. The splitting peaks at 169.9 eV (S $2p_{1/2}$) and 168.7 eV (S $2p_{3/2}$) are from the O=S=O group in the $TFSI^-$ residue. The other pair of peaks at 162.5 eV (S $2p_{1/2}$) and 161.3 eV (S $2p_{3/2}$) represent MgS from the decomposition of $TFSI^-$ with higher intensity in the pure Mg electrolyte.[39] The XPS results demonstrate that although the decomposition of $TFSI^-$ is inevitable, Adding $Na^+$ cation indeed improves the cathodic stability of the $Mg(TFSI)_2$ electrolyte at the anode interface. A trace amount of metallic Na and Na fluoride was also detected in the XPS Na 1s spectrum from the Mg deposition in the Mg/Na electrolyte (**Figure S4** in the Supporting Information), providing additional support to the validation of our hypothesis.

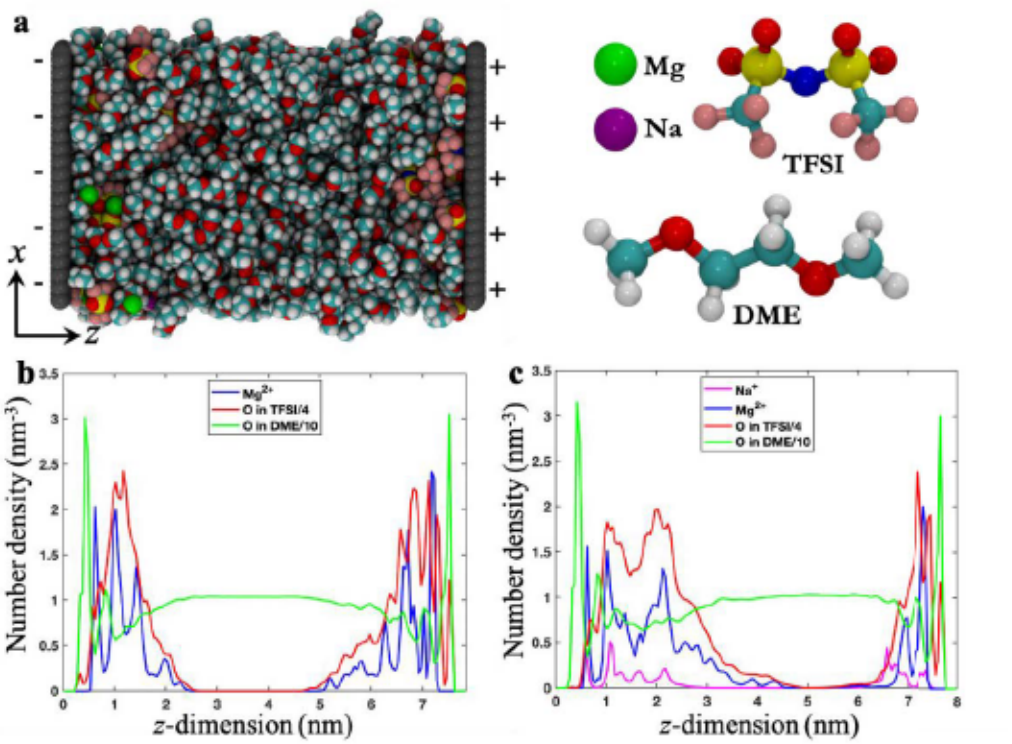


**Figure 3.** (a) Schematic of the simulation system composed of a slab of $Mg(TFSI)_2$/NaTFSI electrolyte sandwiched between two charged electrodes. Green, purple, red, yellow, blue, pink, and cyan spheres denote Mg, Na, O, S, N, F, and C, respectively; Number density profiles of the $Na^+$ ion, $Mg^{2+}$ ion, the oxygen atom of $TFSI^-$ ion and DME molecule in the (b) pure Mg electrolyte and (c) Mg/Na electrolyte. The density of oxygen atoms of $TFSI^-$ ion and DME molecule is divided by a factor of 4 and 10, respectively.

The mechanism of the high cathodic stability of the Mg/Na electrolyte on Mg anode is theoretically examined by MD simulation. A schematic of the simulation box is shown in **Figure 3a**, which consists of two electrodes and a slab of liquid electrolytes (Mg/Na electrolyte is shown). The electrodes measure 4.68 × 4.91 nm$^2$ in the *xy*-plane, and the distance between two electrodes is 7.85 and 8.00 nm for the Mg and Mg/Na electrolytes, respectively. The distance is wide enough to produce a bulk-like condition in the middle of the system.[24, 40] The number of salt and solvent

molecules packed between the electrodes was determined based on the density of the electrolytes calculated in the pre-test MD simulations on the corresponding bulk systems under the NPT ensemble. The salt concentrations in the MD simulations are similar to the experimental concentrations. The MD systems setup was summarized in **Table S1** in the Supporting Information. Small partial charges were distributed uniformly on two electrodes to produce a surface charge density of ±0.03 C $m^{-2}$. The potential drop across the electrolytes is ~2 V (see **Figure S5** in the Supporting Information for details), which is similar to the experimental equilibrium potential (i.e., ~1.5 V). **Figures 3b** and **3c** show the number density profiles of the $Na^+$, $Mg^{2+}$ $TFSI^-$, and DME in the Mg electrolyte and the Mg/Na electrolyte, respectively.

The interface layer immediately adjacent to the negatively charged electrode ($z$ = ~0.5 nm) is composed of DME molecules in both electrolytes. It is worth noting that a small amount of $TFSI^-$ anions exist in this layer in the pure Mg electrolyte. The first cation layer ($z$ = ~0.63 nm) at the interface in the Mg/Na electrolyte is composed of both $Mg^{2+}$ and $Na^+$ cation with a lower number density of $Mg^{2+}$ comparing to that layer in the pure Mg electrolyte. Coincidentally, the number density of $TFSI^-$ anion in the first valley of cation distribution (i.e. $z$ = ~0.80 nm) in the Mg/Na electrolyte is much less than that in the Mg electrolyte. This is the evidence to the mechanism that incorporating $Na^+$ cation in the cation layer can effectively screen $TFSI^-$ anions from the interface. These key features near the negatively charged surface are also captured in the MD simulation with the Madrid-2019 force fields[25] as shown in **Figure S6** in the Supporting Information.

The mechanism of exclusion of $TFSI^-$ anions from the interface at the negatively charged electrode in the Mg/Na electrolyte can be rationalized through density functional theory (DFT) calculation. MD simulation reveals that the interfacial $Na^+$ and $Mg^{2+}$ ions (i.e., ions within the first cation layer near the negatively charged electrode) are mainly coordinated by one and two $TFSI^-$

ions, respectively (see **Figure S7** in the Supporting Information for details). Therefore, we optimized the geometries of $Na^+$-TFSI$^-$ and $Mg^{2+}$-2TFSI$^-$ ion pairs in DFT. We found that a $Na^+$ cation can bond with two oxygen atoms and one fluorine atom from one TFSI$^-$ anion, while a $Mg^{2+}$ ion can bond with four oxygen atoms from two TFSI$^-$ ions to form the most stable adsorption structure in the gas phase (**Figures 4a1** and **4b1**). The bonding distance between $Na^+$ and TFSI$^-$ is larger than that between $Mg^{2+}$ and TFSI$^-$. Meanwhile, the bonding strength of $Na^+$-TFSI$^-$ is significantly weaker than that of the $Mg^{2+}$-2TFSI$^-$. Even after implicit continuum solvents are included in the model, the larger bonding distance and weaker bonding for the $Na^+$-TFSI$^-$ pair compared to the $Mg^{2+}$-TFSI$^-$ pair remain (cf. **Figures 4a2** and **4b2**). These observations are mainly due to the smaller ionic radius of $Mg^{2+}$ ions, which leads to stronger ion-ion electrostatic interactions. Therefore, when $Na^+$ cation takes the place of $Mg^{2+}$ at the electrode interface, fewer TFSI$^-$ anions tend to be attracted to the interface.

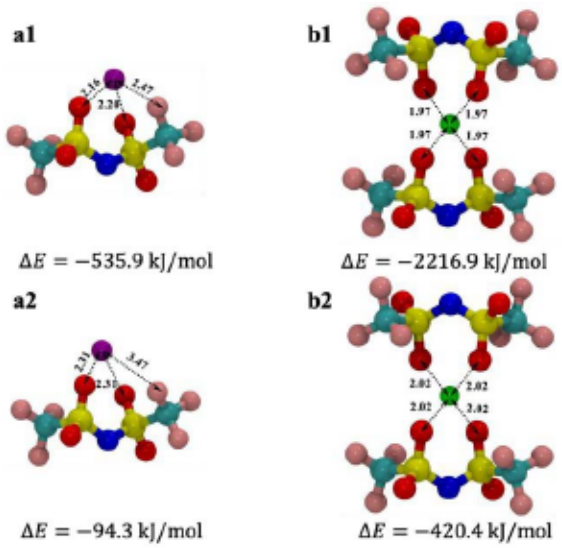


**Figure 4.** Optimized structure of (a1, a2) Na-TFSI and (b1-b2) Mg-2TFSI from the B3LYP/6-31G(d,p) method at (a1, b1) gas phase and (a2, b2) CPCM continuum model. The unit of distance is Å.

## CONCLUSION

Through electrochemical analyses combined with microscopic and spectroscopic characterizations and computational study, we reveal that the addition of $Na^+$ cations in the $Mg(TFSI)_2$ electrolyte has changed the interfacial structure and deposition mechanism for the Mg anode. $Na^+$ cations will be incorporated into the double layer while replacing a certain population of $Mg^{2+}$. Consequently, fewer $TFSI^-$ anions are attracted to the interface due to the weaker electrostatic attraction from the $Na^+$ cation. As a result, the cathodic decomposition of $TFSI^-$ during Mg deposition, a persistent challenge for Mg(TFSI)s electrolyte, can be alleviated. Moreover, the incorporation of $Na^+$ cation into the interfacial layer enables a new mechanism of Mg deposition: Na can be deposited due to the overpotential and then Mg can be chemically deposited by the swift reduction of $Mg^{2+}$ by Na. We believe that this study would provide new insight for better understanding the interface science as well as suggest new interface engineering approaches to design more efficient multivalent ion electrolytes.

## Supporting Information

Mg deposition potential curves at 1 mA $cm^{-2}$; SEM images of Mg deposition at 1 mA $cm^{-2}$; EDX spectra of Mg deposition; Na 1s XPS spectrum of Mg deposition; Calculated distribution of electrical potential in the electrolyte; MD simulation of the number density profiles with the Madrid-2019 force fields; Calculated coordination number of $TFSI^-$ ions and DME molecules around the interfacial $Mg^{2+}$ and $Na^+$ cations; Radial distribution functions from Mg/Na to the oxygen atoms of $TFSI^-$ ions and DME molecules; Table of MD systems studied in this work.

## AUTHOR INFORMATION

## Corresponding Author

Lei Cheng, Email: leicheng@anl.gov
Chunmei Ban, Email: Chunmei.BAN@colorado.edu
Juchen Guo, Email: jguo@engr.ucr.edu

## Notes

The authors declare no competing financial interest.

## ACKNOWLEGEMENTS

X. W. and J. G. acknowledge the support from the U. S. National Science Foundation through grant DMR-2004497. This research was partially supported by the Joint Center for Energy Storage Research (JCESR), a U.S. Department of Energy, Energy Innovation Hub. We thank the Laboratory Computing Resource Center at Argonne National Laboratory for the generous allocation of computing time on the Bebop cluster. XPS was performed at the UC Irvine Materials Research Institute (IMRI) using instrumentation funded in part by the National Science Foundation Major Research Instrumentation Program under grant no. CHE-1338173.

## REFERENCES

1. Attias, R.; Salama, M.; Hirsch, B.; Goffer, Y.; Aurbach, D., Anode-Electrolyte Interfaces in Secondary Magnesium Batteries. *Joule* **2019,** *3* (1), 27-52.

2. Shi, J.; Zhang, J.; Guo, J.; Lu, J., Interfaces in rechargeable magnesium batteries. *Nanoscale Horizons* **2020,** *5* (11), 1467-1475.

3. Gregory, T. D.; Hoffman, R. J.; Winterton, R. C., Nonaqueous electrochemistry of magnesium: applications to energy storage. *J. Electrochem. Soc.* **1990,** *137* (3), 775.

4. Shterenberg, I.; Salama, M.; Gofer, Y.; Aurbach, D., Hexafluorophosphate-Based Solutions for Mg Batteries and the Importance of Chlorides. *Langmuir* **2017,** *33* (37), 9472-9478.

5. McArthur, S. G.; Geng, L.; Guo, J.; Lavallo, V., Cation reduction and comproportionation as novel strategies to produce high voltage, halide free, carborane based electrolytes for rechargeable Mg batteries. *Inorganic Chemistry Frontiers* **2015,** *2* (12), 1101-1104.

6. McArthur, S. G.; Jay, R.; Geng, L.; Guo, J.; Lavallo, V., Below the 12-vertex: 10-vertex carborane anions as non-corrosive, halide free, electrolytes for rechargeable Mg batteries. *Chem. Commun.* **2017,** *53* (32), 4453-4456.

7. Dong, H.; Tutusaus, O.; Liang, Y.; Zhang, Y.; Lebens-Higgins, Z.; Yang, W.; Mohtadi, R.; Yao, Y., High-power Mg batteries enabled by heterogeneous enolization redox chemistry and weakly coordinating electrolytes. *Nature Energy* **2020**, 1-8.

8. Jay, R.; Tomich, A. W.; Zhang, J.; Zhao, Y.; De Gorostiza, A.; Lavallo, V.; Guo, J., Comparative Study of Mg(CB11H12)2 and Mg(TFSI)2 at the Magnesium/Electrolyte Interface. *ACS Appl. Mater. Interfaces* **2019,** *11* (12), 11414-11420.

9. Zhao-Karger, Z.; Liu, R.; Dai, W.; Li, Z.; Diemant, T.; Vinayan, B. P.; Bonatto Minella, C.; Yu, X.; Manthiram, A.; Behm, R. J.; Ruben, M.; Fichtner, M., Toward Highly Reversible Magnesium–Sulfur Batteries with Efficient and Practical Mg[B(hfip)4]2Electrolyte. *ACS Energy Letters* **2018,** *3* (8), 2005-2013.

10. Zhang, Z.; Cui, Z.; Qiao, L.; Guan, J.; Xu, H.; Wang, X.; Hu, P.; Du, H.; Li, S.; Zhou, X.; Dong, S.; Liu, Z.; Cui, G.; Chen, L., Novel Design Concepts of Efficient Mg-Ion Electrolytes

toward High-Performance Magnesium-Selenium and Magnesium-Sulfur Batteries. *Adv. Energy Mater.* **2017,** *7* (11).

11. Rajput, N. N.; Qu, X.; Sa, N.; Burrell, A. K.; Persson, K. A., The coupling between stability and ion pair formation in magnesium electrolytes from first-principles quantum mechanics and classical molecular dynamics. *J. Am. Chem. Soc.* **2015,** *137* (9), 3411-20.

12. Shterenberg, I.; Salama, M.; Yoo, H. D.; Gofer, Y.; Park, J.-B.; Sun, Y.-K.; Aurbach, D., Evaluation of (CF3SO2)2N−(TFSI) Based Electrolyte Solutions for Mg Batteries. *J. Electrochem. Soc.* **2015,** *162* (13), A7118-A7128.

13. Son, S. B.; Gao, T.; Harvey, S. P.; Steirer, K. X.; Stokes, A.; Norman, A.; Wang, C.; Cresce, A.; Xu, K.; Ban, C., An artificial interphase enables reversible magnesium chemistry in carbonate electrolytes. *Nat Chem* **2018,** *10* (5), 532-539.

14. Giffin, G. A.; Moretti, A.; Jeong, S.; Passerini, S., Complex Nature of Ionic Coordination in Magnesium Ionic Liquid-Based Electrolytes: Solvates with Mobile Mg2+ Cations. *J. Phys. Chem. C* **2014,** *118* (19), 9966-9973.

15. Borodin, O.; Giffin, G. A.; Moretti, A.; Haskins, J. B.; Lawson, J. W.; Henderson, W. A.; Passerini, S., Insights into the Structure and Transport of the Lithium, Sodium, Magnesium, and Zinc Bis(trifluoromethansulfonyl)imide Salts in Ionic Liquids. *J. Phys. Chem. C* **2018,** *122* (35), 20108-20121.

16. Firdaous, L.; Malériat, J. P.; Schlumpf, J. P.; Quéméneur, F., Transfer of monovalent and divalent cations in salt solutions by electrodialysis. *Sep. Sci. Technol.* **2007,** *42* (5), 931-948.

17. Zeng, J.; Cao, Z.; Yang, Y.; Wang, Y.; Peng, Y.; Zhang, Y.; Wang, J.; Zhao, J., A long cycle-life Na-Mg hybrid battery with a chlorine-free electrolyte based on Mg(TFSI)2. *Electrochim. Acta* **2018,** *284*, 1-9.

18. Hess, B.; Kutzner, C.; Van Der Spoel, D.; Lindahl, E., GROMACS 4: algorithms for highly efficient, load-balanced, and scalable molecular simulation. *Journal of chemical theory and computation* **2008,** *4* (3), 435-447.

19. Parrinello, M.; Rahman, A., Polymorphic transitions in single crystals: A new molecular dynamics method. *Journal of Applied physics* **1981,** *52* (12), 7182-7190.

20. Nosé, S.; Klein, M., Constant pressure molecular dynamics for molecular systems. *Molecular Physics* **1983,** *50* (5), 1055-1076.

21. Jorgensen, W. L.; Maxwell, D. S.; Tirado-Rives, J., Development and testing of the OPLS all-atom force field on conformational energetics and properties of organic liquids. *Journal of the American Chemical Society* **1996,** *118* (45), 11225-11236.

22. Doherty, B.; Zhong, X.; Gathiaka, S.; Li, B.; Acevedo, O., Revisiting OPLS force field parameters for ionic liquid simulations. *Journal of chemical theory and computation* **2017,** *13* (12), 6131-6145.

23. Cornell, W. D.; Cieplak, P.; Bayly, C. I.; Gould, I. R.; Merz, K. M.; Ferguson, D. M.; Spellmeyer, D. C.; Fox, T.; Caldwell, J. W.; Kollman, P. A., A second generation force field for the simulation of proteins, nucleic acids, and organic molecules. *Journal of the American Chemical Society* **1995,** *117* (19), 5179-5197.

24. Yu, Z.; Fang, C.; Huang, J.; Sumpter, B. G.; Qiao, R., Solvate Ionic Liquids at Electrified Interfaces. *ACS Appl. Mater. Interfaces* **2018,** *10* (38), 32151-32161.

25. Zeron, I.; Abascal, J.; Vega, C., A force field of Li+, Na+, K+, Mg2+, Ca2+, Cl−, and SO 4 2− in aqueous solution based on the TIP4P/2005 water model and scaled charges for the ions. *The Journal of chemical physics* **2019,** *151* (13), 134504.

26. Bussi, G.; Donadio, D.; Parrinello, M., Canonical sampling through velocity rescaling. *The Journal of chemical physics* **2007,** *126* (1), 014101.

27. Yeh, I.-C.; Berkowitz, M. L., Ewald summation for systems with slab geometry. *The Journal of chemical physics* **1999,** *111* (7), 3155-3162.

28. Cossi, M.; Rega, N.; Scalmani, G.; Barone, V., Energies, structures, and electronic properties of molecules in solution with the C-PCM solvation model. *Journal of computational chemistry* **2003,** *24* (6), 669-681.

29. Frisch, M.; Trucks, G.; Schlegel, H. B.; Scuseria, G. E.; Robb, M. A.; Cheeseman, J. R.; Scalmani, G.; Barone, V.; Mennucci, B.; Petersson, G., gaussian 09, Revision d. 01, Gaussian. *Inc., Wallingford CT* **2009,** *201*.

30. Cheng, L.; Redfern, P.; Lau, K. C.; Assary, R. S.; Narayanan, B.; Curtiss, L. A., Computational studies of solubilities of LiO2 and Li2O2 in aprotic solvents. *Journal of The Electrochemical Society* **2017,** *164* (11), E3696.

31. Su, H.; Fu, C.; Zhao, Y.; Long, D.; Ling, L.; Wong, B. M.; Lu, J.; Guo, J., Polycation Binders: An Effective Approach toward Lithium Polysulfide Sequestration in Li–S Batteries. *ACS Energy Letters* **2017,** *2* (11), 2591-2597.

32. Aurbach, D.; Lu, Z.; Schechter, A.; Gofer, Y.; Gizbar, H.; Turgeman, R.; Cohen, Y.; Moshkovich, M.; Levi, E., Prototype systems for rechargeable magnesium batteries. *Nature* **2000,** *407* (6805), 724-727.

33. Griffin, J. M.; Forse, A. C.; Tsai, W. Y.; Taberna, P. L.; Simon, P.; Grey, C. P., In situ NMR and electrochemical quartz crystal microbalance techniques reveal the structure of the electrical double layer in supercapacitors. *Nat. Mater.* **2015,** *14* (8), 812-9.

34. Mosch, H. L.; Akintola, O.; Plass, W.; Hoppener, S.; Schubert, U. S.; Ignaszak, A., Specific Surface versus Electrochemically Active Area of the Carbon/Polypyrrole Capacitor: Correlation of Ion Dynamics Studied by an Electrochemical Quartz Crystal Microbalance with BET Surface. *Langmuir* **2016,** *32* (18), 4440-9.

35. Ley, L.; McFeely, F.; Kowalczyk, S.; Jenkin, J.; Shirley, D., Many-body effects in x-ray photoemission from magnesium. *Phys. Rev. B* **1975,** *11* (2), 600.

36. Da-Ming, S.; Zhao-Qi, S.; Ai-Xia, L.; Zhi-Yuan, X., Oxidation behaviour of MgF2 in Ag–MgF2 cermet. *Vacuum* **1999,** *55* (1), 39-44.

37. Gao, T.; Hou, S.; Huynh, K.; Wang, F.; Eidson, N.; Fan, X.; Han, F.; Luo, C.; Mao, M.; Li, X.; Wang, C., Existence of Solid Electrolyte Interphase in Mg Batteries: Mg/S Chemistry as an Example. *ACS Appl. Mater. Interfaces* **2018,** *10* (17), 14767-14776.

38. Morgan, W. E.; Van Wazer, J. R.; Stec, W. J., Inner-orbital photoelectron spectroscopy of the alkali metal halides, perchlorates, phosphates, and pyrophosphates. *JACS* **1973,** *95* (3), 751-755.

39. Ding, M. S.; Diemant, T.; Behm, R. J.; Passerini, S.; Giffin, G. A., Dendrite Growth in Mg Metal Cells Containing Mg(TFSI)2/Glyme Electrolytes. *J. Electrochem. Soc.* **2018,** *165* (10), A1983-A1990.

40. Zhao, W.; Bi, S.; Balke, N.; Rack, P. D.; Ward, T. Z.; Kalinin, S. V.; Dai, S.; Feng, G., Understanding Electric Double-Layer Gating Based on Ionic Liquids: from Nanoscale to Macroscale. *ACS Appl. Mater. Interfaces* **2018,** *10* (49), 43211-43218.